Numerical study of swirling and non-swirling annular impinging jets with heat transfer

Thomas Hallqvist* and Laszlo Fuchs†

This paper deals with numerical simulation of annular impinging jets with heat transfer by means of Large Eddy Simulation (LES). The LES code uses higher order finite-differences on staggered Cartesian non-uniform grids. The current LES have the potential of dealing with transition as well as providing data on details of larger scale structures, statistical correlations and turbulent spectral content. The impinging annular jet has a nozzle-to-plate spacing equal to 2 nozzle diameters and the Reynolds number is 23800. The ratio between the inner and outer diameter is 0.4. Three different swirl numbers are considered, ranging from non-swirling to strongly swirling flow. From the LES results the transition process in the jet is clearly detected. The annular configuration as well as the applied swirl strongly influences the development of the flow field. With swirl the wall heat transfer rates becomes obstructed. This is primarily due to the spreading of the jet resulting in low axial momentum within the center region. Compared to the circular impinging jet the annular configuration features higher levels of turbulence within the stagnation region. This is, due to the restrained axial momentum, of great importance for the wall heat transfer.

Nomenclature

C, c	Normalized mean and instantaneous scalar concentration/temperature
C_f	Mean wall friction coefficient
C_0	Characteristic concentration/temperature at nozzle outlet, K
D, d	Normalized outer and inner diameter of the annular nozzle
D_0	Characteristic length scale, m
f	Frequency, Hz
H	Normalized distance from nozzle outlet to impingement wall
k	Normalized turbulent kinetic energy
k_0	Characteristic turbulent kinetic energy at nozzle outlet, m^2/s^2
Nu	Mean Nusselt number
p	Normalized pressure
Re	Reynolds number ($V_0 D_0/\nu$)
S	Swirl number
St	Strouhal number (fD_0/V_0)
t	Normalized time
U_i, u_i	Normalized mean and instantaneous velocity (U, V, W, u, v, w)
V_0	Characteristic velocity at nozzle outlet, m/s
x_i	Cartesian coordinate (x, y, z)
Greek Letters	
ν	Kinematic viscosity, m^2/s

*Ph.D. student, Royal Institute of Technology, Dept. of Mechanics, Stockholm, Sweden. e-mail: thom@mech.kth.se
†Professor of Fluid Mechanics, Lund Institute of Technology, Lund, Sweden

I. Introduction

With the impinging jet configuration high heat or mass transfer rates are efficiently achieved. Therefore, the impinging jet is widely used in industrial applications. Common application areas are cooling of electrical components and gas turbines combustion chambers. It is also used in processing of metal and glass. Most studies of impinging jets are related to simplified geometries as compared to practical applications. This is so since much of the physics is captured also in the simplest case (flat impingement wall). Effects of particular details of the application (such as swirl, curved impingement walls) may be studied separately and thereby expose the effects of these parameters. The wall heat transfer rate depends strongly on a number of parameters. For instance the ratio between the characteristic height and diameter of the jet and the character of the incoming jet flow. Studies of annular impinging jets are important for, among other things, axial fan applications. Due to the annular configuration the axial mass flow is restrained, particularly in the proximal region of the axial jet. Hence, the heat transfer rates close to the stagnation point ought to be heavily obstructed. However, the outcome of this feature strongly depends on the nozzle outlet boundary conditions and the nozzle-to-plate spacing.

For large enough nozzle-to-plate spacing (H/D), the initial state of the impinging jet is characterized by a free jet. A free jet can be defined as a jet entering a large chamber containing a quiescent fluid. The shear-layer grows in size in the downstream direction. This is due to vortex roll-up, initiated by the inherent shear layer instability. The roll-up results in considerable entrainment of ambient fluid into the jet. Due to the radial spreading of the jet, the axial velocity decreases continuously in the streamwise direction. Initially, if the disturbance level is very small, the shear-layer instability can be described by Kelvin-Helmholtz linear stability theory, as the flow features a laminar main flow with superimposed random fluctuations and a point of inflection. A common process in the free axial jet is the, so called, vortex pairing process. This process depends strongly on the character of the initial flow field as shown by, among others, Hwang et al.[1] Vortex pairing occurs when two closely located structures have grown large enough that they coalesce. The resulting larger vortex is, within this work, named primary vortex. Primary vortices are alternatingly shed within the axial shear layer.

There are relatively few articles written on annular impinging jets. At the present time no articles have been found on swirling annular impinging jets. However, Chattopadhyah[2] performed numerical work on laminar annular impinging jets. They found that the heat transfer for the annular configuration was 20 percent lower compared to a circular configuration featuring the same mass flow rate at the nozzle outlet. Also Maki & Yabe[3] performed heat transfer studies of annular impinging jets. Studies of acoustic excited annular impinging jets where performed by Travnicek & Vaclav.[4] One of their objectives was to study the influence from excitation on the impingement wall heat/mass transfer rates. They found, with respect to the size of the recirculation zone, two different regimes of the impinging jet. The near wall recirculation has large influence on the wall heat transfer.

Contrary to studies of annular impinging jets, there are numerous work done on non-swirling circular impinging jets. Among others, Liu & Sullivan[5] studied the influence from turbulent separation, induced by strong secondary vortices, on wall heat transfer. Related work were performed by Hwang et al.,[1] who applied control of the formation of vortices and studied the influence on wall heat transfer. Influence from different nozzle outlet velocity profiles were studied by Behnia et al.[6] Studies of swirling circular impinging jets have been conducted by among others Huang & El-Genk.[7] They studied the influence on wall heat transfer for different swirl levels. Experimental work on swirling circular impinging jets where conducted by Lee et al.[8]

A subject with several similarities to the study of swirling impinging jets, is the study of vortex breakdown for free jets. For a free swirling jet there are several different modes or states of breakdown. As shown by Sarpkaya[9] the first breakdown appears as an axisymmetric recirculation bubble. Hereafter the flow stabilizes and then breaks down, a second time, into a helical shape. Billant et al.[10] studied the characteristics of various breakdown states. They identified four distinct forms of vortex breakdown. In conjunction to the shear layer instability there may also be contribution from centrifugal instability as the azimuthal velocity distribution of the swirling jet satisfies the Rayleigh criterion.[10]

II. Governing Equations

The motion of fluids is fully described by the continuity equation and the Navier Stokes equations. The latter ones are, in dimensionless form, written as

$$\frac{\partial u_i}{\partial t} + \frac{\partial}{\partial x_j}(u_i u_j) = -\frac{\partial p}{\partial x_i} + \frac{1}{Re}\frac{\partial}{\partial x_j}\frac{\partial u_i}{\partial x_j}. \tag{1}$$

With the assumption of temperature being a passive scalar, *i.e.* does not influence the velocity field, the following transport equation can be used to predict heat transfer

$$\frac{\partial c}{\partial t} + u_j\frac{\partial c}{\partial x_j} = \Gamma\frac{\partial}{\partial x_j}\frac{\partial c}{\partial x_j}, \tag{2}$$

where Γ is the diffusivity and c is the concentration of the passive scalar. The scalar is referred to as conserved since there is no sink or source term in the transport equation above. As c corresponds to temperature, Γ represents thermal diffusivity, commonly referred to as α, and ν/α is the Prandtl number.

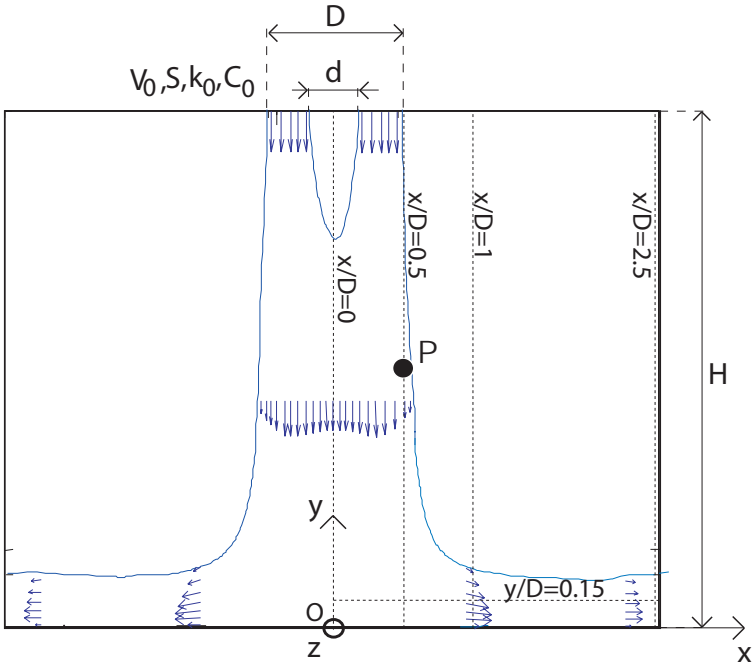

Figure 1. Cross-section of the impinging jet.

III. Turbulence Modeling and Numerics

To fully describe a turbulent flow, all scales of motion, from the largest energetic scales to the smallest Kolmogorov scales must be resolved. The computational requirement for resolving all the scales of the Navier Stokes equations is out of reach for more complex geometries. If one is interested in the dynamics of the flow and/or when the RANS framework is inadequate one may use Large Eddy Simulations. In LES one resolves the larger eddies and model the effects of the small (unresolved) scales on the resolved ones. The cut-off wave number is determined by the filter function. In this work the numerical scheme acts as a filter, with the filter size being proportional to the grid size. The code is based on a staggered Cartesian grid and for the discretization finite differences are used. To avoid masking of the Sub-Grid-Scale (SGS) stress by the truncation error high order schemes are needed. The spatial discretization of the momentum equation uses a $\mathcal{O}(h^4)$ central differences scheme for all terms except the advection term which is approximated by a $\mathcal{O}(h^3)$ upwind scheme, proposed by Rai & Moin.[11] The discretization of the advection term adds enough dissipation to allow implicit SGS modeling, as verified by among others Olsson & Fuchs[12] and Revstedt.[13] In this work no explicit SGS model has been employed.

On average, the amount of (turbulent) energy in the small scales is independent of the numerical dissipation, provided that one can resolve a portion of the inertial subrange. Thus, by having adequate resolution the numerical dissipation does not affect the large-scale results. If there is excessive numerical dissipation, a posteriori analysis of the turbulent energy spectrum would show a non-existing inertial subrange. In the near wall region, the grid is highly resolved (using grid stretching). There are several grid nodes in the viscous sublayer. For this reason, the no-slip condition is applied at the impingement wall, without any further attempt to add damping or using "wall functions". For the temporal discretization a time splitting scheme has been employed.[12]

IV. Problem Setup

The present study features an annular jet emanating from a nozzle into a large space limited by the impingement and the confinement wall. In Fig. 1 the cross-section of the impinging jet is shown. The confinement wall is located at the upper horizontal line, so also the nozzle outlet (*i.e.* velocity inlet). The impingement wall is located at the lower horizontal line, *i.e.* where $y/D = 0$. The outer and inner diameter of the nozzle is defined by D and d, respectively. H is the height of the geometry and letters with subscripts "0" are the characteristic parameters for the present configuration. The dotted lines represent evaluation lines. The nozzle features a flat axial velocity profile, V_0, with superimposed random disturbances, k_0. The corresponding velocity for the circular impinging jet is $V_0\prime$ (calculated as $V_0(1-d^2/D^2)$). The swirl-number, S, is defined as the azimuthal velocity, U_s, at the periphery of the nozzle divided by $V_0\prime$. Three different swirl numbers are considered, namely $S = 0$ (*Case1*), $S = 0.5$ (*Case2*) and $S = 1$ (*Case3*). Solid body rotation is applied and the concentration as well as the velocities are set to zero at the impingement and the confinement wall. If nothing else is mentioned appropriate combinations of D_0, $V_0\prime$ and C_0 are used to normalize the results. The Reynolds number is defined as $Re = V_0 D_0/\nu$ and equals 23800 in order to asses the mass flow of the circular impinging jet ($Re = V_0\prime D_0/\nu = 20000$).

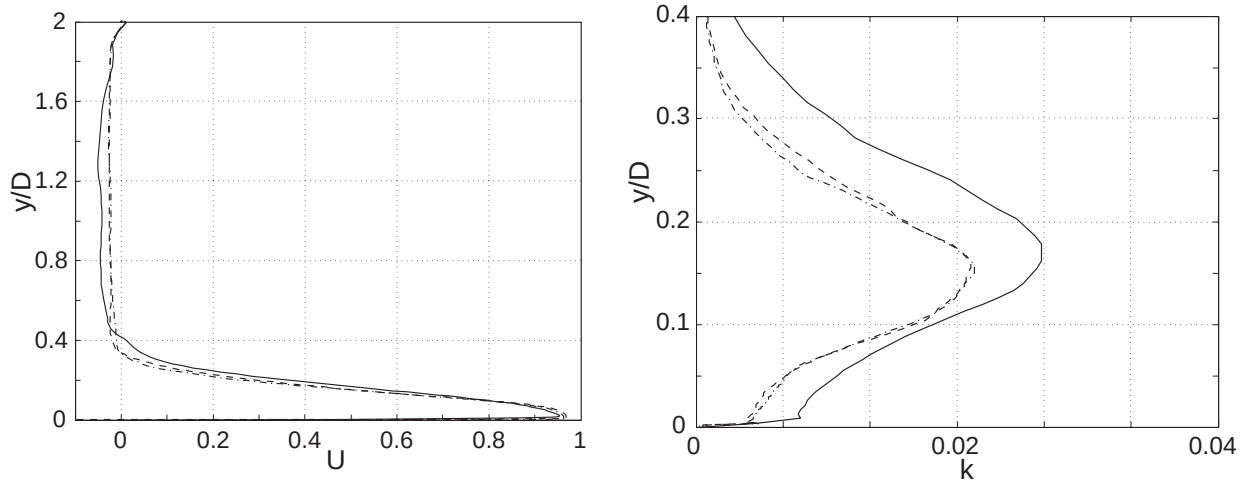

(a) Mean radial velocity, U, at $x/D = 1$.

(b) Turbulent kinetic energy, k, at $x/D = 1$.

Figure 2. Evaluation of grid dependency. (—): 194x98x194 (*grid1*), (- - -): 194x146x194 (*grid2*), (- · -): 194x226x194 (*grid3*).

As a complement to the comprehensive study of model behavior and grid dependency (for the present code) performed by Olsson[14] and Revstedt,[13] three different grids have been studied (circular impinging jet configuration). These have $194 * 98 * 194$ (*grid1*), $194 * 146 * 194$ (*grid2*) and $194 * 226 * 194$ (*grid3*) cells, respectively, on the finest out of five multi-grid levels. As verified by Fig. 2(a) and Fig. 2(b), the average deviation between the two finer grids is negligible. In the present work *grid2* has been employed.

V. Results

A. Basic Features of Impinging Jets

In the present configuration, the nozzle outlet velocity profile is, as defined above, flat. But as the flow is convected downstream the influence from the surrounding quiescent fluid results in a strong axial shear layer, both in the outer and the inner region of the annular jet. The axisymmetric shear layer is inherently unstable and initially symmetrical disturbances are dominant. These disturbances correspond to the linear stability theory of a two-dimensional shear-layer (*i.e.* Kelvin Helmholtz instability) and implies that disturbances grow exponentially in the downstream direction. Slightly downstream of the nozzle, non-linear effects become important and the linear approximation breaks down. Even further downstream there is a process featuring merging of vortices, that results in strong, so called, primary vortices, and halving of the characteristic frequency. This feature, however, depends strongly on the inlet conditions, such as the disturbance and swirl levels.

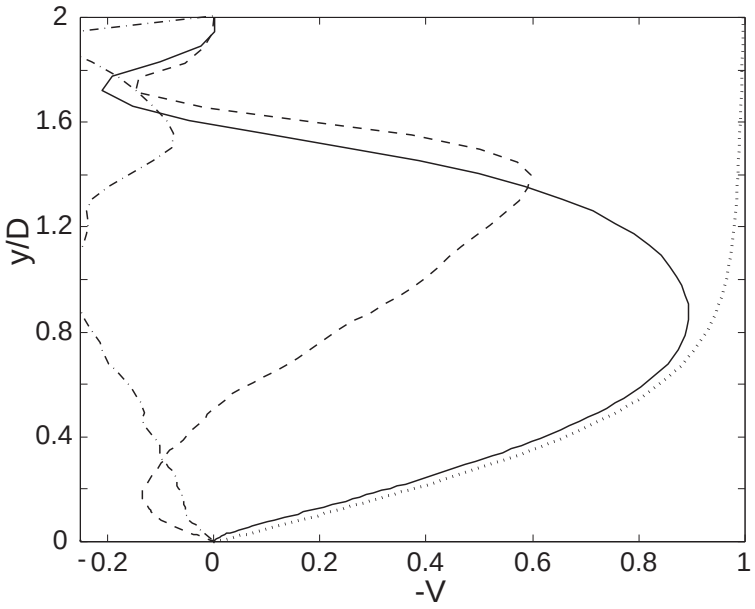

Figure 3. Mean axial velocity decay along the stagnation line. (—): *Case1* $S = 0$, (- - -): *Case2* $S = 0.5$, (- · -): *Case3* $S = 1$, (· · ·): $S = 0$ circular impinging jet.[15]

B. Mean Flow Character

The mean axial velocity decay along the stagnation line is depicted in Fig. 3. For comparison results from the circular impinging jet study by Hallqvist & Fuchs[15] has been included. The annular configuration has as expected large influence on the flow character along the stagnation line. For the non-swirling annular jet the result, in the near wall region, is similar to that for the circular jet. This is so since the character of the axial jet in the near wall region resembles of a circular one. This feature is coupled to, among other things, the nozzle-to-plate spacing and the swirl level. Close to the nozzle outlet there is, as depicted by the negative axial velocity, a recirculation region. When swirl is added the character of the axial flow changes. For *Case2* there is an additional recirculation region close to the wall. The near wall recirculation was also observed in the study of swirling circular impinging jets.[16] With a swirl number of $S = 0.5$ the circular jet does not feature backflow, however as the swirl number equals $S = 1$ the circular jet exhibits larger recirculation region as compared to the annular *Case3*.

The downstream development of the wall jet is depicted in Fig. 4. The radial velocity, U, at $x/D = 1$ is depicted in Fig. 4(a) and at $x/D = 2.5$ in Fig. 4(b). Results from the circular impinging jet[15] and experimental results by Cooper et al.[17] are included. As depicted by Fig. 4(a) the velocity for the three non-swirling cases are similar. The annular nozzle has thus only weak influence on the flow field at this downstream location. As the swirl level increases the wall jet becomes wider in similar manner as for the

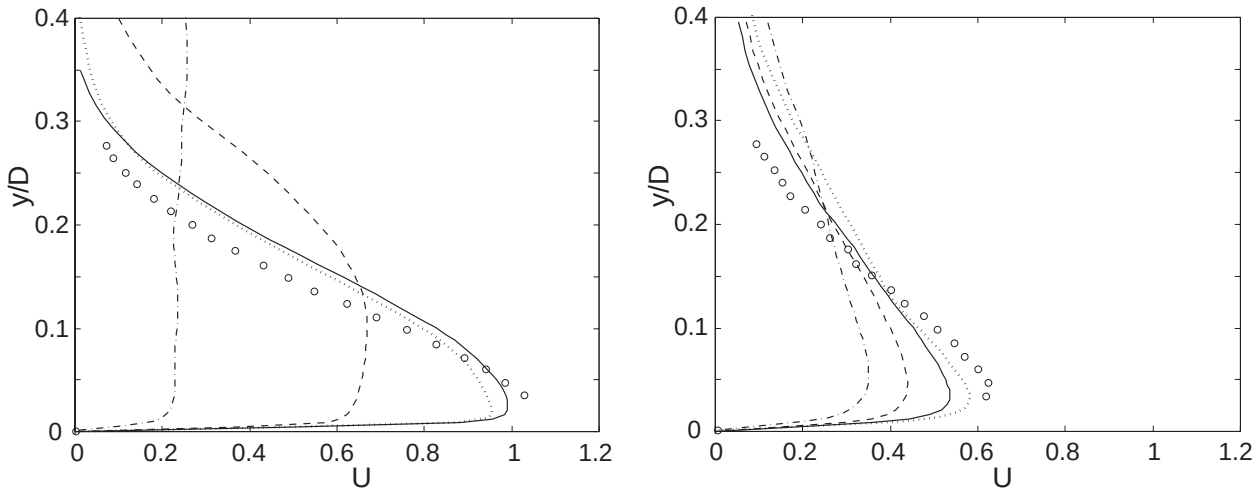

(a) Radial velocity at $x/D = 1$.

(b) Radial velocity at $x/D = 2.5$.

Figure 4. Wall normal distribution of the mean radial velocity, U. (—): *Case1* $S = 0$, (- - -): *Case2* $S = 0.5$, (- · -): *Case3* $S = 1$, (···): $S = 0$ circular impinging jet,[15] (○): $S = 0$ experimental data of circular impinging jet.[17]

swirling circular jet.[16] Further downstream at $x/D = 2.5$ the radial velocity is, as depicted in Fig. 4(b), significantly lower. This is caused by the continuous entrainment of ambient fluid (wider profile) and, of course, by the increase in section area. The influence from swirl is not as pronounced as in Fig. 4(a). Contrary to the other cases *Case3* exhibits higher maximum velocity at $x/D = 2.5$. This is a direct consequence of the spreading of the axial jet.

The recirculation regions predicted by the annular jet configuration are qualitatively depicted by the mean friction coefficient, C_f, in Fig. 5. On average, *Case1* does not exhibit flow separation. Compared to the circular impinging jet C_f is overall lower. In *Case2* the flow attaches the wall at approximately $x/D = 0.65$ and in *Case3* at approximately $x/D = 0.7$. As depicted the maximum in backflow is obtained at a swirl number lower than unity, as *Case2* features larger negative values relative to *Case3*. Downstream of $x/D = 1.5$ the character of the wall jet is similar for all cases. The recirculation within the stagnation region has, as will be shown later, negative influence on wall heat transfer.

Qualitative representations of the flow field are depicted in Fig. 6. Velocity vectors for *case1* are shown in Fig. 6(a), for *Case2* in Fig. 6(b) and for *Case3* in Fig. 6(c). For *Case1* the annularity of the jet persists downstream to $y/D = 1.4$. This location is, on average, the lower limit of the recirculation region. Downstream from here the axial jet resembles much of a circular jet. When swirl is added the spreading of the axial jet increases. *Case2* also features "circular jet behavior", however in more limited region. This is so since a second recirculation region is formed downstream of $y/D = 0.8$. For *Case3* the axial jet experiences strong spreading which results in coalescence of the upper and lower recirculation regions. The influence from swirl on the wall jet is clearly depicted by the relative length and distribution of the velocity vectors.

C. Turbulence Characteristics

As shown by Hallqvist & Fuchs[16] the turbulence level within the axial jet for the circular configuration increases as swirl is applied. Also for the annular configuration the turbulent kinetic energy increases with increased level of swirl. As depicted in Fig. 7 the growth rate from the nozzle outlet and downstream is as strongest for *Case3*. The increase of k continues downstream to $y/D = 1$. For the two other cases the growth is weaker and limited to the proximal region of the jet. The strong growth of k for *Case3* is attributed to the intense azimuthal shear layer and the strong jet spreading (contrary to the other two cases, both the inner and outer shear layers plus the bulk flow of the axial jet influences k for $y/D > 1$ in Fig. 7).

The turbulence level within the wall jet is depicted in Fig. 8 by means of the radial perturbation velocity, u_{rms}. In Fig. 8(a) u_{rms} at $x/D = 1$ is shown and in Fig. 8(b) at $x/D = 2.5$. For the circular impinging jet the strongly swirling case ($S = 1$) featured the highest level of u_{rms} at $x/D = 1$. However, for the annular configuration *Case3* does not exhibit the highest level of u_{rms}, at least in the wall jet region. This

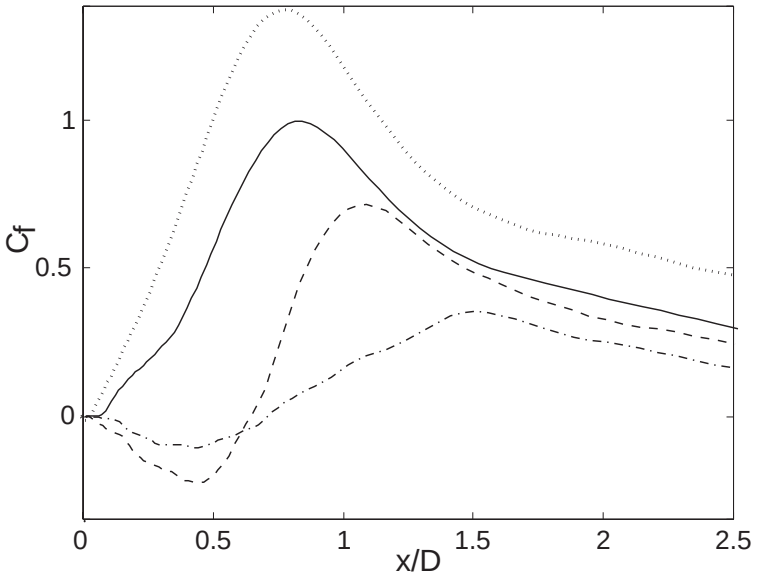

Figure 5. Mean friction coefficient, C_f. Data normalized by the maximum value of *Case1*. (—): *Case1* $S = 0$, (- - -): *Case2* $S = 0.5$, (- · -): *Case3* $S = 1$, (···): $S = 0$ circular impinging jet.[15]

is related to the location of flow attachment. In the strongly swirling circular case the flow attached the wall (on average) at $x/D = 1$, which resulted in locally high fluctuation levels. *Case1* and *Case2* predict similar distribution of u_{rms} featuring two local maximums, however the magnitudes differ strongly. Further downstream at $x/D = 2.5$ the results resemble of those for the circular jet. Characterized by relatively low level of u_{rms} for *Case3*, whereas, for *Case1* and *Case2* u_{rms} is higher and of similar character.

The wall parallel development of k is depicted in Fig. 9. Compared to the circular jet, that featured close to zero level of turbulence in the stagnation region, the annular configuration show overall high levels. This is an important issue regarding wall heat transfer as the annular jet features low axial momentum in the center region of the jet. Further downstream, where the influence from the inlet conditions are weak the annular configuration shows the same behavior as the circular impinging jet.

D. Structures and Dynamics

A common characteristic for non-swirling circular jets is distinct formation of periodic structures.[15] Also, as swirl is added[16] the circular impinging jet features both distinct natural and subharmonic frequencies. The power spectrums for the u-velocity component at the point labeled "P" in Fig. 1 are presented in Fig. 10. As depicted *Case1* features a natural frequency, St_n, of 1.5 and a subharmonic, St_s, of 0.75 (characterizes the formation of primary vortices). For the circular jet the corresponding frequencies were 1.4 and 0.7, respectively. As compared to *Case1* the natural frequency for *Case2* is slightly lower and contains greater amount of energy. However, *Case2* does not show any clear subharmonic. For the highly swirling *Case3* no distinct frequencies are observed.

The downstream development of the characteristic frequencies along the evaluation line located at $x/D = 0.5$ are depicted in Fig. 11. The result for *Case1* is depicted in Fig. 11(a). As shown the natural frequency is dominant from, approximately, the nozzle outlet and downstream to $y/D = 1.2$. At this location there is vortex pairing that results in halving of the frequency, *i.e.* formation of a subharmonic. The subharmonic persists downstream to $y/D = 0.6$. In *Case2* (Fig. 11(b)) the natural frequency becomes dominant slightly further downstream as compared to *Case1*. The frequency of the natural mode is lower and equals 1.4. Furthermore, there is no distinct vortex pairing. Also for *Case3* there is a natural mode present, but only in a limited region close to the nozzle outlet. Judging from the velocity vectors shown in Fig. 6 the implication of the $x/D = 0.5$ evaluation line differs for the three cases. This is so since for high level of swirl the jet spreading is strong and, thus, the vortical structures that are formed and convected within the outer shear layer are not completely traced. Relative to *Case1* the spectrums for *Case2* and *Case3* are greater influenced by the more stable (with respect to periodic structures) bulk flow and, also, by the chaotic

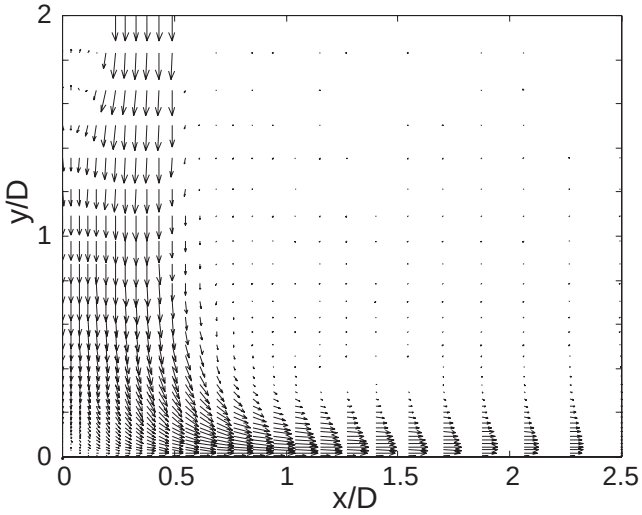

(a) *Case1* S=0.

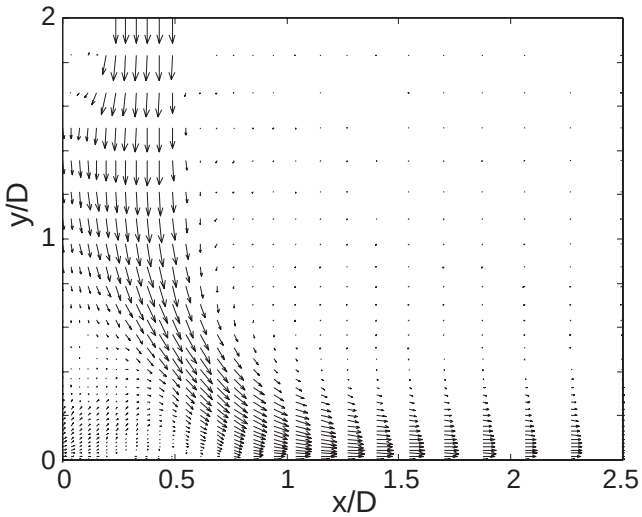

(b) *Case2* S=0.5.

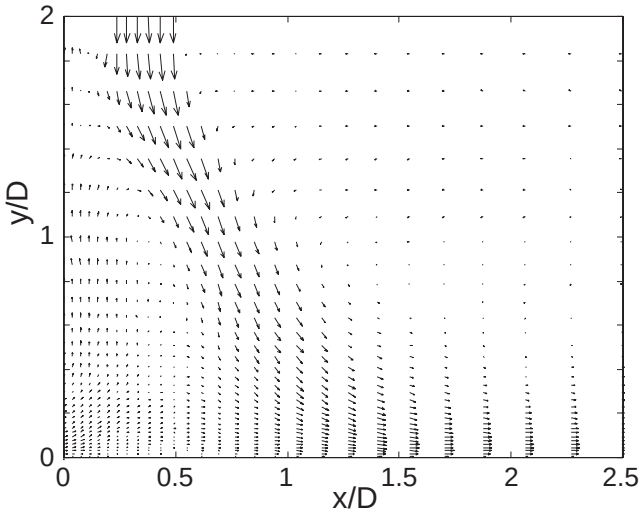

(c) *Case3* S=1.

Figure 6. Velocity vectors in the xy-plane.

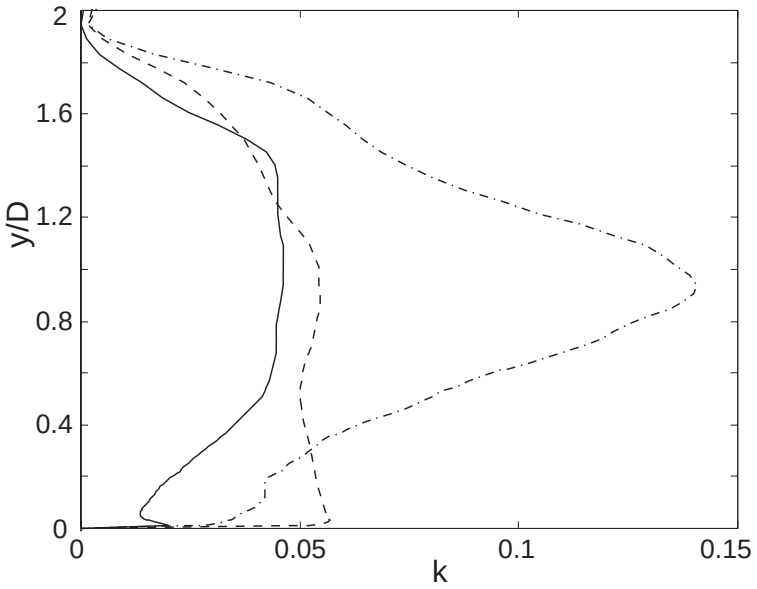

Figure 7. Wall normal distribution of the turbulent kinetic energy, k, along $x/D = 0.5$. (—): *Case1* $S = 0$, (- - -): *Case2* $S = 0.5$, (- · -): *Case3* $S = 1$.

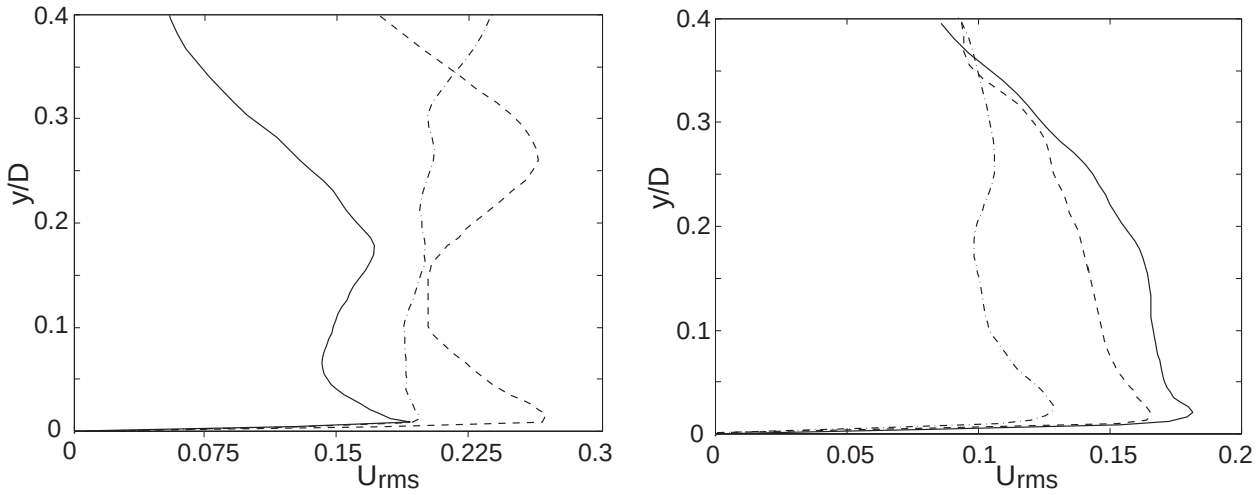

(a) Root mean square velocity at $x/D = 1$.

(b) Root mean square velocity at $x/D = 2.5$.

Figure 8. Wall normal distribution of the radial perturbation velocity, u_{rms}. (—): *Case1* $S = 0$, (- - -): *Case2* $S = 0.5$, (- · -): *Case3* $S = 1$.

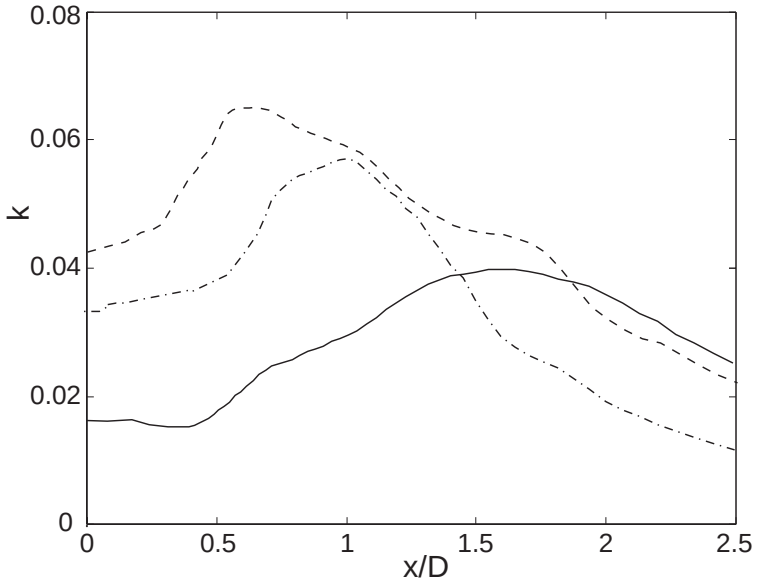

Figure 9. Wall parallel development of the turbulent kinetic energy, k, at $y/D = 0.15$. (—): *Case1* $S = 0$, (- - -): *Case2* $S = 0.5$, (- · -): *Case3* $S = 1$.

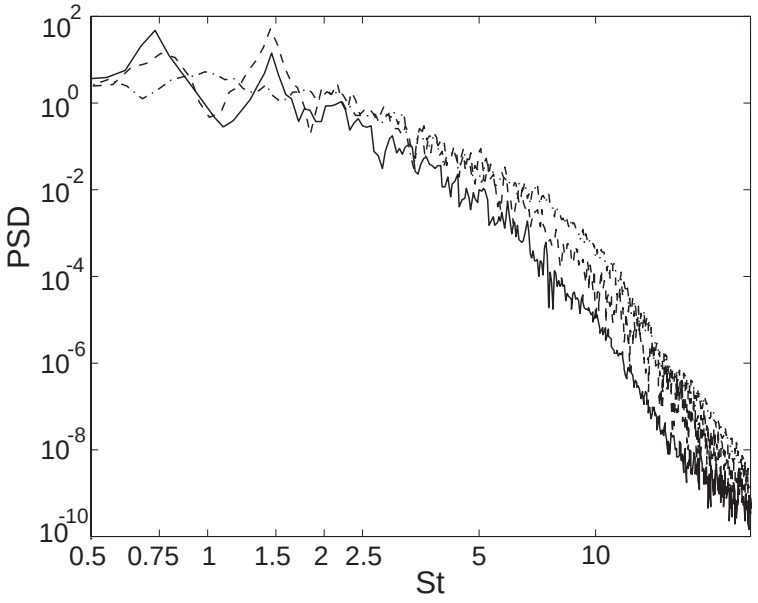

Figure 10. Power Spectral Density (PSD) for u at point P ($x/D = 0.5$, $y/D = 1$). (—): *Case1* $S = 0$, (- - -): *Case2* $S = 0.5$, (- · -): *Case3* $S = 1$.

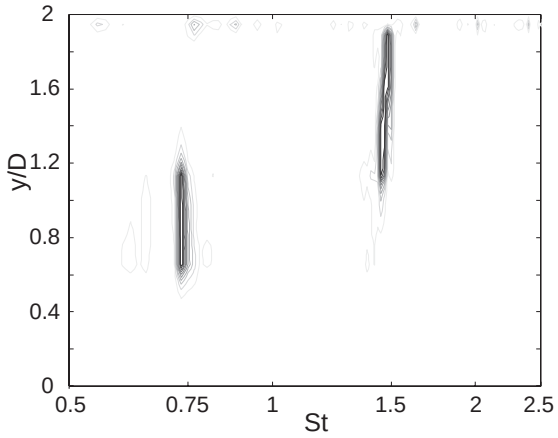

(a) *Case1* S=0.

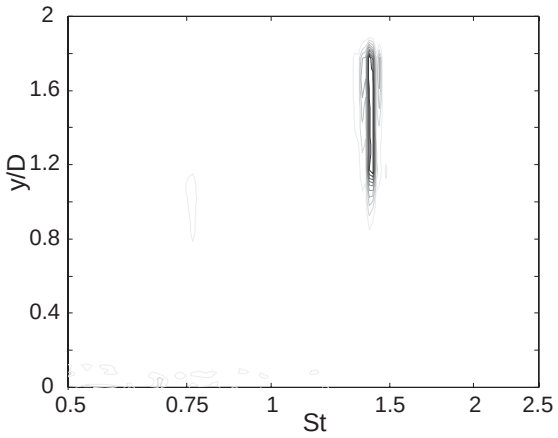

(b) *Case2* S=0.5.

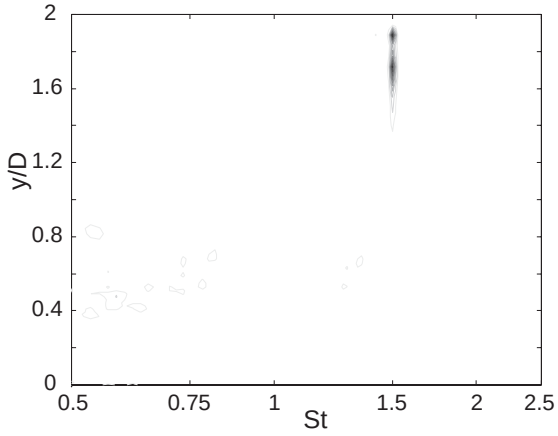

(c) *Case3* S=1.

Figure 11. Space frequency map for u along the $x/D = 0.5$ evaluation line.

recirculation region. Hence, the shortage of dominant scales.

E. Heat Transfer

To achieve high heat or mass transfer is commonly the major objective of impinging jets. As discussed by Hallqvist & Fuchs[16] the Nusselt number within the stagnation region decreases with increased level of swirl. This despite the increase in turbulence level. To understand the nature of wall heat transfer the scalar distribution within the entire domain is of importance.

The distribution of C at $x/D = 1$ is depicted in Fig. 12(a) and at $x/D = 2.5$ in Fig. 12(b). The transport of the scalar is influenced by all three velocity components. This is why C does not experience the same strong influence from swirl as the radial velocity component does. This is evident when comparing Fig. 12(a) and Fig. 4(a). However, for increasing level of swirl the distribution of C at $x/D = 1$ becomes smeared out. This has great influence on the Nusselt number, as Nu is proportional to the wall normal derivative of C. At $x/D = 2.5$ all three cases show similar distribution in the near wall region. Further out in the wall jet, *Case3* exhibits the highest level of C.

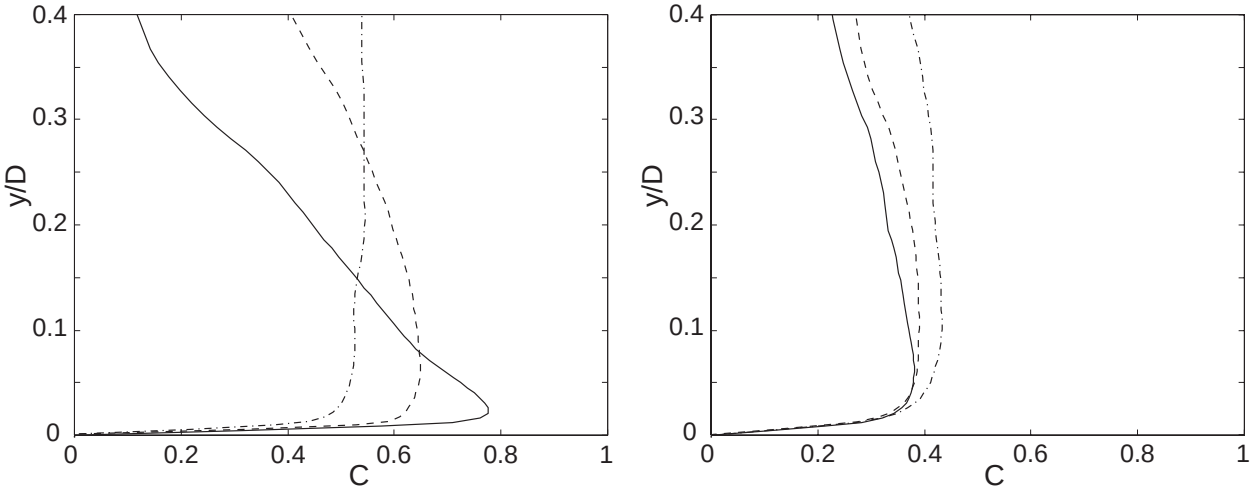

(a) Scalar concentration at $x/D = 1$.

(b) Scalar concentration at $x/D = 2.5$.

Figure 12. Wall normal distribution of the mean scalar concentration, C. (—): *Case1* $S = 0$, (- - -): *Case2* $S = 0.5$, (- · -): *Case3* $S = 1$.

The distribution of the mean Nusselt number is depicted in Fig. 13. For a circular jet, the first peak is commonly attributed to a local thinning of the velocity boundary layer. The second peak is commonly claimed to be due to induced interacting vortices (secondary vortices) between the large-scale vortices (primary vortices) and the impingement wall and by transition from a laminar to a turbulent wall jet.[18] As depicted in the figure the Nusselt number for $x/D < 1.4$ decreases with increased level of swirl. Downstream of $x/D = 1.4$ the results for the three annular cases are almost identical. In the stagnation region the level of Nu for *Case1* is similar to that for the circular impinging jet.[16] An explanation to the comparable levels of heat transfer may be that the level of k within the stagnation region is higher for the annular configuration as compared to the circular. The main problem with an annular nozzle configuration is, as mentioned before, that the momentum is low in the center region of the axial jet. However, as verified, the high levels of k compensates for this drawback.

VI. Conclusions

Basic studies of the dynamical character of the annular impinging jet have been performed, both for non-swirling and swirling jets. With high level of swirl the axial jet experiences strong spreading, whereas, the non-swirling annular jet shows, more or less, same behavior as the circular jet. The results show that swirl has a negative effect on wall heat transfer within the stagnation region. This is so despite the higher turbulence level as compared to the non-swirling case. However, relative to swirling circular impinging jets

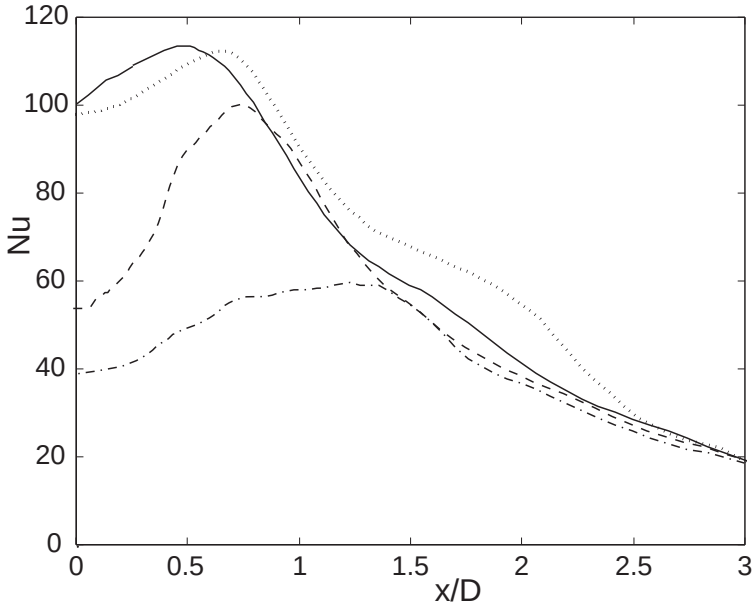

Figure 13. Mean Nusselt number, Nu**. (—):** ***Case1*** $S = 0$**, (- - -):** ***Case2*** $S = 0.5$**, (- · -):** ***Case3*** $S = 1$**, (· · ·):** $S = 0$ **circular impinging jet.**[15]

the annular configuration show same level of heat transfer. This is due to the relative high turbulence level within the stagnation region. Further analysis will be conducted with emphasis on the influence from grid resolution and nozzle outlet conditions.

References

[1]Hwang, S.D., Lee, C.H. and Cho, H.H., "Heat transfer and flow structures in axisymmetric impinging jet controlled by vortex pairing," *Int. J. Heat and Fluid Flow*, Vol. 22, 2001, pp. 293–300.

[2]Chattopadhyah, H., "Numerical investigation of heat transfer from impinging annular jet," *Int. J. Heat Mass Transfer*, Vol. 47, 2004, pp. 3197–3201.

[3]Maki, H. and yabe, A., "Heat transfer by the annular impinging jet," *Exp. Heat Transfer*, Vol. 2, 1989, pp. 1–12.

[4]Travnicek, Z. and Vaclav, T., "Annular impinging jet with recirculation zone expanded by acoustic excitation," *Int. J. Heat Mass Transfer*, Vol. 47, 2004, pp. 2329–2341.

[5]Liu, T. and Sullivan, J. P., "Heat transfer and flow structures in an excited circular impinging jet," *Int. J. Heat Mass Transfer*, Vol. 39, 1996, pp. 3695–3706.

[6]Behnia, M., Parneix, S., Shabany, Y. and Durbin, P.A., "Numerical study of turbulent heat transfer in confined and unconfined impinging jets," *Int. J. Heat and Fluid Flow*, Vol. 20, 1999, pp. 1–9.

[7]Huang, L. and El-Genk, M.S., "Heat transfer and flow visualization experiments of swirling, multi-channel, and conventional impinging jets," *Int. J. Heat Mass Transfer*, Vol. 41, 1998, pp. 583–600.

[8]Lee, D. H., Won, S. Y., Kim, Y. T. and Chung, Y. S., "Turbulent heat transfer from a flat surface to a swirling round impinging jet," *Int. J. Heat Mass Transfer*, Vol. 45, 2002, pp. 223–227.

[9]Sarpkaya, T., "On stationary and traveling vortex breakdowns," *J. Fluid. Mech.*, Vol. 45, 1971, pp. 545-559.

[10]Billant, P., Chomaz, J.-M. and Huerre, P., "Experimental study of vortex breakdown in swirling jets," *J. Fluid. Mech.*, Vol. 376, 1998, pp. 183–219.

[11]Rai, M. M. and Moin, P., "Direct simulation of turbulent flow using finite difference schemes," *J. Comput. Phys.*, Vol. 96, 1991, pp. 15–35.

[12]Olsson, M. and Fuchs, L., "Large eddy simulation of a forced semi-confined circular impinging jet," *Phys. Fluids*, Vol. 10, 1998, pp. 476–486.

[13]Revstedt, J., "On the modeling of Turbulent Flow and Mixing in Stirred Reactors," Doctoral Thesis, Division of Heat Transfer, Department of Heat and Power Engineering, Lund Institute of Technology, Lund, 1999.

[14]Olsson, M., "Large Eddy Simulation of Turbulent Jets," Doctoral Thesis 1999:16, Dept. Mechanics, Royal Institute of Technology, Stockholm, 1997.

[15]Hallqvist, T. and Fuchs, L., "Numerical study of impinging jets-I. Flow field characteristics," Submitted for publication.

[16]Hallqvist, T. and Fuchs, L., "Numerical study of swirling impinging jets with heat transfer," HT-FED2004, ASME Summer Conference, 2004.

[17]Cooper, D. and Jackson, D. and Launder, B. and Liao, G., "Impinging jet studies for turbulence model assessment-I. Flow field experiments," *Int. J. Heat Mass Transfer*, Vol. 36, 1993, pp. 2675–2684.
[18]Hallqvist, T. and Fuchs, L., "Numerical study of impinging jets-II. Mixing characteristics," Submitted for publication.